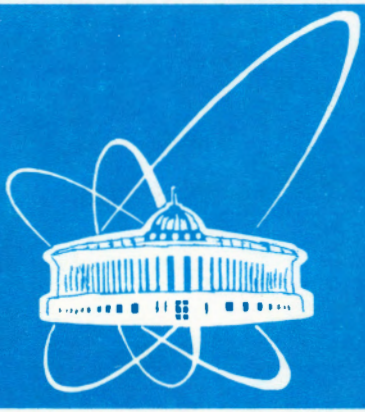

сообщения
объединенного
института
ядерных
исследований
дубна

E6-94-271

A.Anastassov, Yu.P.Gangrsky, B.N.Markov,
S.G.Zemlyanoi, K.P.Marinova[1], E.G.Nadjakov[1],
B.K.Kul'djanov[2]

NUCLEAR STRUCTURE BY LASER SPECTROSCOPY

[1]Faculty of Physics, University of Sofia, Sofia, Bulgaria
[2]Institute of Nuclear Physics, Uzbek Academy of Sciences,
Tashkent, Uzbekistan

1994

1. Introduction

The study of isotope shifts (IS) and hyperfine structure (hfs) of optical transitions in atomic spectra has been an important source of information on nuclear electric and magnetic moments from the very beginnings of nuclear physics. IS yield detailed information about the changes in the radial moments of the nuclear charge distribution between isotopes, and the hfs allows accurate measurements of electric and magnetic moments of the nucleus. Very precise measurements are even capable of yielding information about changes in the nuclear magnetization distribution between isotopes. The relation between nuclear parameters and experimentally measured IS and hfs in the atomic spectra is demonstrated briefly in fig. 1.

The laser spectroscopy is a modern variant of the classical optical spectroscopy which has had a major impact on studies of basic nuclear properties historically. The developement of dye lasers with their:

- high power density: > 10 mW/cm^2, corresponding to photon beam intensity $> 10^{17}$ cm^{-2}s^{-1}
- high spectral resolution: laser linewidth of the order of 1 MHz
- perfect collimation: divergence < 20 mrad
- tunability in large spectral range: $\approx 300 - 800$ nm

revitalized the study of the optical spectra of atoms as a source

NUCLEUS: ELECTRON SHELL:

I : spin

μ_I : magnetic dipole moment J : intrinsic quantum number

Q_s : electric quadrupole moment W_J: energy of atomic level

$\langle r^2 \rangle$: ms charge radius υ : optical transition energy

Nucleus - electron shell interaction:	hyperfine splitting isotope shift

HYPERFINE SPLITTING

$$|J-I| \leq F \leq |J+I|$$

$$\Delta W_F = A\frac{C}{2} + B\,\frac{3C(C+1) - 4I(I+1)J(J+1)}{8I(2I-1)J(2J-1)}$$

$$A = \frac{\mu_I\,\overline{H(0)}}{IJ} \qquad B = eQ_s\overline{\varphi_{JJ(0)}}$$

ΔW_F : experimentally measured quantity from hfs

$\overline{H(0)}$, $\overline{\varphi_{JJ}(0)}$: theoretically calculated quantities, depending only on electron shell

μ_I, Q_s : nuclear parameters determined from hfs

ISOTOPE SHIFT

$$\delta\upsilon^{A'A} = \upsilon^{A'} - \upsilon^{A} = \delta\upsilon^{A'A}_{FS} + \delta\upsilon^{A'A}_{MS}$$

field shift: FS $\quad \delta\upsilon_{FS} = E_i f(Z)\lambda \cong E_i f(Z)\delta\langle r^2\rangle$

mass shift : MS $\quad \delta\upsilon_{MS} = M_i\,\frac{A' - A}{A'A}$

$\delta\upsilon^{A'A}$: experimentally measured IS

$\delta\upsilon_{MS}$, E_i : theoretically calculated or empirically determined quantities, depending only on the electron shell properties

$f(Z)$: relativistic and nuclear correction to E_i: tabulated

λ, $\delta\langle r^2\rangle$: nuclear parameters determined from IS

Fig. 1 Relation between nuclear and atomic properties

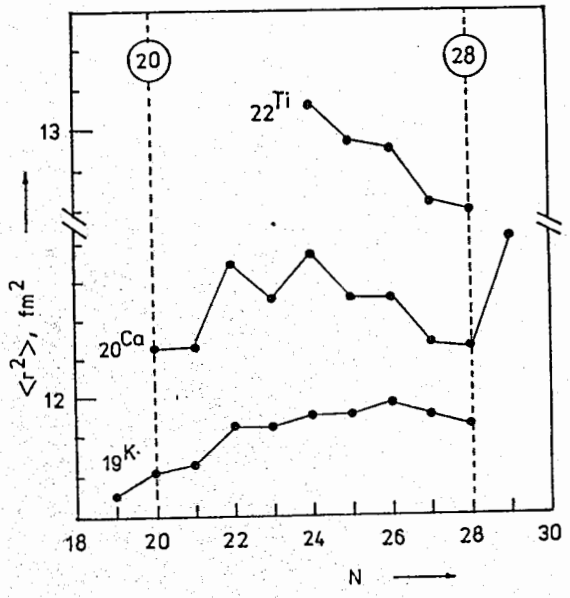

Fig. 2 Absolute values of ms nuclear charge radii $\langle r^2\rangle$ versus neutron number N in light nuclei region: proton number Z around Z = 20

of nuclear information. The contemporary laser spectroscopic methods with their high resolution and high sensitivity offer the following possibilities in nuclear physics:

i) high accuracy in determination of nuclear moments and nuclear shape by high accurasy measurements of hfs and IS in the atomic spectra;

ii) observation of extremely small quantities of materials up to single atoms and ions;

iii) investigation of long chains of short lived nuclei in ground and isomeric states not only off-line, but also on-line, with low production rate.

Thus the problem how to get access to the basic nuclear ground

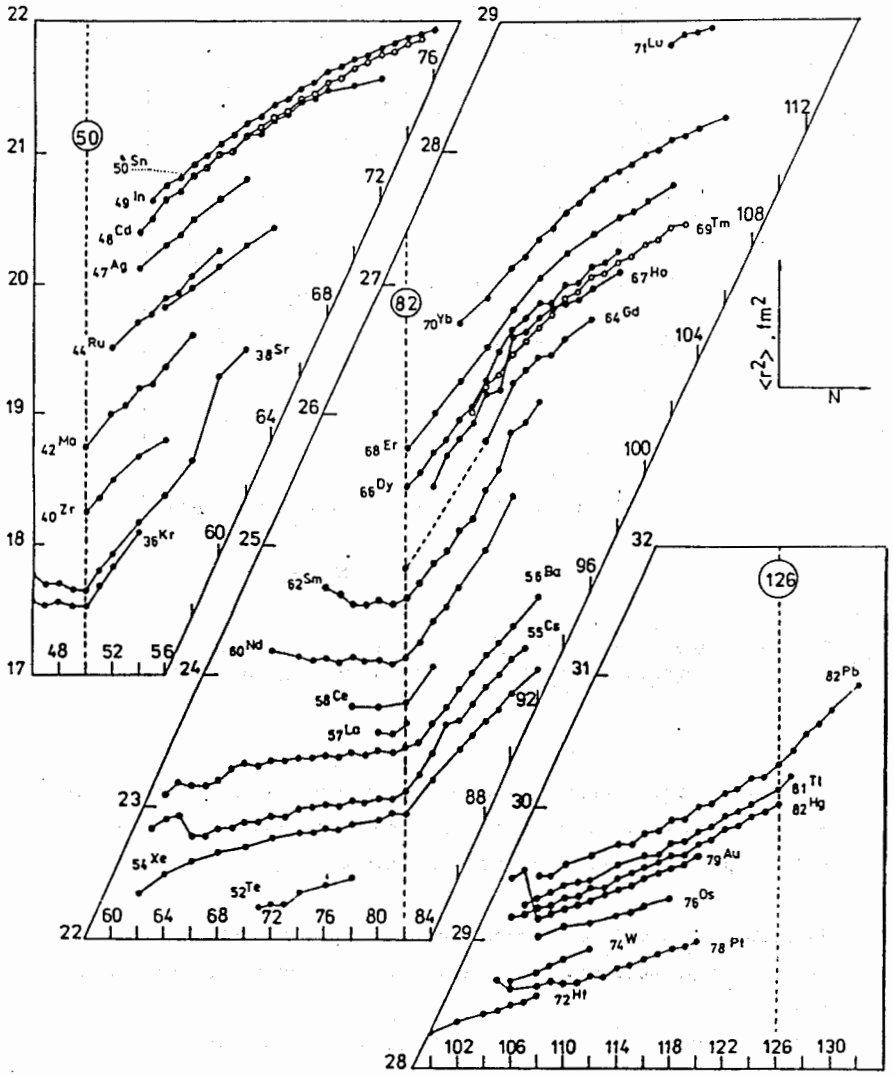

Fig. 3 Isotopic nuclear radii absolute values: ms radius $\langle r^2 \rangle$ versus neutron number N at various proton number Z

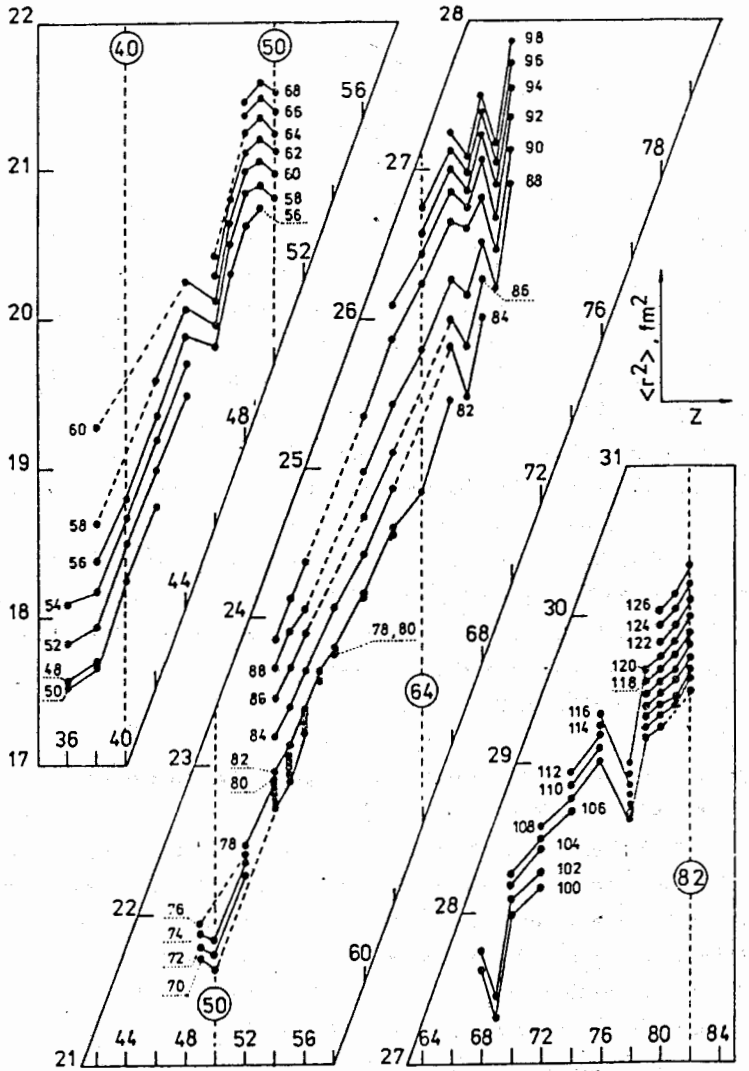

Fig. 4 Isotonic nuclear radii absolute values: ms radius $\langle r^2 \rangle$ versus proton number Z at various neutron number N

and isomeric state properties (spins, moments, charge radii) has been solved in an efficient and unique way. Laser spectroscopic experiments have been performed in the last years on a large amount of nuclides (> 400) with half-life down to 1 ms and production rate down to 10^4 s.

The compilations shown in figs. 2, 3 and 4 represent nowadays knowledge about nuclear charge radii. Fig.2 and fig.3 display the mean square (ms) charge radii versus the neutron number N of the isotopes at various proton number Z and fig.4 - versus the proton number Z at various neutron number N. This nuclear radii systematics will be discussed in detail below. Here we emphasize the rather irregular changes of neighbouring nuclei, revealing pronounced nuclear structure effects.

This paper illustrates the contribution of laser spectroscopy to our knowledge about nuclear structure properties, in particular about variations of nuclear charge radii in long isotopic and isotonic chains comprising stable and short lived isotopes (part 2). Finally, the recent results obtained experimentally in the Flerov Laboratory of Nuclear Reactions JINR, Dubna, are presented and discussed (part 3).

2. General trends of variations in nuclear ms charge radii

2.1 Nuclear charge radii systematics

The nuclear charge radius, as one of the most obvious and important nuclear parameters, gives information about shell model and effective interaction influence on nuclear structure. Therefore it has been treated in many experiments of two types. The first type yields data on ms absolute charge radii $\langle r^2 \rangle$, the second type - on ms charge radii changes $\delta\langle r^2 \rangle$.

A great number of experimental results on $\langle r^2 \rangle$ or $\langle r^2 \rangle^{1/2}$ respectively, are reviewed in [1, 2] from electron scattering experiments and in [3] from muonic atom spectra. The values of $\langle r^2 \rangle$ obtained in the various experiments are in most cases internally consistent [4] even though the model independence of such analysis is still questionable. Compilations of experimental absolute charge radii measured by fast electron scattering and muonic atom X-rays have been published recently

[5, 6]. They cover many elements ranging from $_1$H to $_{95}$Am, but refer to a low number of stable (or nearly stable: Th - Am) isotopes.

On the other hand using high resolution and high sensitivity laser spectroscopic techniques, high accuracy data on $\delta\langle r^2 \rangle$ for extended chains of isotopes and isomers of many elements have been obtained. Review tables of $\delta\langle r^2 \rangle$, including ranges far from stability, are presented in the systematics [7, 8]. Important consequences are discussed in several papers: [9].

A combined analysis of both type data on $\langle r^2 \rangle$ and $\delta\langle r^2 \rangle$ has been performed to yield ms charge radii for extended nuclear chains with high accuracy [10, 11]. It may be applied to those elements for which both types of data exist. The extension of their neutron number regions and thus of their isotopic radius chains is determined by the region of $\delta\langle r^2 \rangle$ data.

Since absolute radii values have been fitted, the systematics can be presented from two points of view: as isotopic nuclear radii systematics (figs. 2,3), but also as isotonic nuclear radii systematics (fig. 4). Four effects are evident.

The first effect is that the slope of the curves $\langle r^2(Z) \rangle$ in fig. 4 is considerably steeper than the slope of the curves $\langle r^2(N) \rangle$ in fig. 3. This is naturally explained by the additional Coulomb interaction between protons with respect to the interaction between neutrons. It will cause a higher $\langle r^2 \rangle$ increase when protons are added as compared with the situation when neutrons are added.

The second effect is connected with magic numbers. The slope of the curves in both figures is steeper at the beginning of an interval between two magic numbers and tending to saturation at the end. It becomes even negative in fig. 3 before neutron magic numbers 50 and 82 and in fig. 4 - before proton magic number 50. Such slope has been noticed in particular for $N < 82$ and $Z = 54 - 63$ by [12]. This effect is also observed in fig. 4 before proton number 38, which is in agreement with other evidence that 38 might be a proton magic number. The effect is related to filling up a shell before the magic number. We have not included our fit about $_{63}$Eu in the figures because there are doubts about the

experimental data on $\langle r^2 \rangle$. Therefore, as an exception, the model data of [4] have been adopted in the analysis. If these results had been included in the figures, the same pattern would have been observed before proton number 64, but for neutron numbers 89- 91 only. This would be in agreement with other evidence that 64 might be a proton magic number. But we would suggest instead that these experimental data should be reconsidered.

The third effect is the staggering of the curves $\langle r^2(N) \rangle$ in figs. 2,3 and $\langle r^2(Z) \rangle$ in fig. 4, and the fact that this effect is much more pronounced in fig. 4. Here is included an odd-even staggering, causing usually a hole in the curve for odd Z just as for odd N , with some exceptions related to the second effect observed. But especially in the case of $\langle r^2(Z) \rangle$ in fig. 4 an even-even staggering is observed in the region before proton magic number 82. The odd-even staggering might be connected with the pairing interaction.

The fourth effect is the similarity in the shape of the $\langle r^2(N) \rangle$ curves for adjacent Z in figs. 2,3 and much more evident in the $\langle r^2(Z) \rangle$ curves for adjacent N in fig. 4. It is also explained by the shell model: e.g. in the second case the shape of the curve is related to the interaction between protons, and the situation will be changed weakly if neutrons are added to another shell with completely different level energy. This is the effect, in the first case demonstrated with an exact procedure by [9], based on the data of radii changes for eight elements with Z = 80 - 88 (without Z = 85), extended as a general tendency here.

The most interestig features of ms nuclear radii changes in dependence on neutron number N have been treated in many separate papers and also considered in detail in some extended reviews [8]. From the point of view of nuclear structure the following nuclid regions are of particular interest:

- proton closed shell
- neutron closed shell
- transition from spherical to deformed nuclei.

Here they will be described briefly.

2.2 Regions of proton closed shell

Long isotopic chains with proton shell closure are investigated for Z = 20 (Ca), 50 (Sn) and 82 (Pb), and for some neighbouring nuclei (see figs. 2 and 3). The following features can be noted:

$_{20}$Ca:
- IS measurements cover a full neutron shell namely $\nu 1f_{7/2}$;
- the ms charge radius goes through a maximum in the middle of the shell (fig.2);
- the two double-magic nuclei ^{40}Ca and ^{48}Ca have the same ms charge radius, while the electron scattering experiments have revealed that the charge distributions themselves are not identical.

$_{50}$Sn:
- the isotopic chain is located in the middle between the two neutron shell closures N = 50 and N = 82;
- a smooth parabolic dependence $\langle r^2(N) \rangle$ is observed, which can be fitted with good approximation to: $\delta\langle r^2 \rangle = A(66 - N) + B(66 - N)^2$.

$_{82}$Pb:
- the isotopic chain lies around N = 126 neutron shell closure;
- with decreasing N the radii vary more slowly than expected by a naive $A^{1/3}$ law predicted by the most sipmle liquid drop model;
- there is a discontinuity after closing the shell, empirically often related to decreasing binding energy.

In all three cases the overall trends are superimposed by an odd-even staggering, which is a well known feature in all mass regions. The dependences $\langle r^2(N) \rangle$ of the nearest neighbouring nuclei are very similar, e.g. Ca and K; Sn, In and Cd; Pb, Tl and Hg.

Presently the most realistic and simplest global model which attemts to account for the proton rearrangement is the droplet model [8, 13]. It considers the proton and neutron fluids independently; the neutron excess causes a dilatation of the proton distribution. It predicts a constant increase of the nuclear charge volume at constant deformation. In general, however,

the variation of the radii is influenced by possible effects arising from a nonspherical shape, increasing the average radial extension of a nucleus as compared with a spherical nucleus of the same volume.

In what follows, the experimental results on nuclear charge radii will be treated predominantly using the standard droplet model relation

$$\delta\langle r^2\rangle = \delta\langle r^2\rangle_o + (5/4\pi)\langle r^2\rangle_o \Sigma\delta\langle\beta^2\rangle_i \qquad (1)$$

with $\langle r^2\rangle_o$ - the spherical droplet model radius and $\delta\langle\beta^2\rangle$ - the change in the ms deformation of multipolarity i . It allows to account for deformation effects by using empirical nuclear deformations deduced from measured electromagnetic transition probabilities.

The droplet model analysis has been performed for all nuclides mentioned in this section (e.g. see [8] and the references therein) with the assumption of a constant intrinsic skin diffuseness. It describes the data for $_{82}$Pb isotopes fairly well: $\Sigma\delta\langle\beta^2\rangle_i = 0$ seems to be a good assumption for the doubly-magic nucleus ^{208}Pb. The deviations from the straight lines produced by spherical gross models reflect the increasing dynamic collective motion on either side of a magic neutron number. At N < 126 this discrepancy becomes vanishing if the quadrupole deformation parameter β_2 is taken into account in eq.(1). For N > 126 it is known that the octupole strength increases strongly due to the $g_{9/2}$ valence neutrons which have large octupole matrix elements connecting to $\nu j_{15/2}$ states [14]. One could therefore argue that higher multipole deformations contribute in addition to the quadrupole mode and that this contribution steadily increases across the closed shell [8]. We notice that such assumption is only one possible explanation of the experimental results.

The parabolic curve of $\langle r^2\rangle$ in the case of $_{50}$Sn corresponds very well to eq.(1): the first term, describing changes in the spherical shape with adding neutrons, the second - the influence of collective dynamic motion. The quantitative description requires the contribution of two deformation parameters: quadrupole β_2 [15] and octupole β_3 [16].

The astonishing behaviour of $_{20}$Ca nuclear radii is hardly to be explained by eq.(1). The major part of the observed effect can be attributed to collective β_2 and β_3 contributions, but even the addition of ms deformations up to β_5 describes the N-dependence of $\delta\langle r^2\rangle$ only qualitatively. The difference may or may not be interpreted as the residual "non-collective" change of skin thickness [8]. It could be attributed as well to a deficiency of the collective or of the droplet model.

As seen, the N dependence of nuclear charge radii for nuclei with closed proton shell exhibits essential variations: from a curve passing through a maximum for $_{20}$Ca to a straight line for $_{82}$Pb. This can be ascribed to a variation of the contributions of different effects into the nuclear charge distribution. For light elements the influence of the skin thickness and nuclear shape (different orders of deformations) is relatively high, because of their strong change with N. In heavy nuclei the change of the nuclear volume when neutrons are added dominates.

2.3 Regions of neutron closed shell

The systematics of fig. 2 and fig. 3 gives an excellent view on the general peculiarities of $\langle r^2(N)\rangle$ dependence around neutron magic numbers: 20 (fig. 2) and 50, 82, 126 (fig. 3):

- a well pronounced kink at the neutron magic number is observed;
- below the neutron magic number the ms charge radius remains almost constant, above it expands rapidly (nearly twice the rate of the spherical droplet model);
- the slopes of the curves at either side of a given magic number are nearly equal for different elements; their variation with the magic number is neglectingly small, too.

These features are obviously a particular case of the most general effects, mentioned in section 2.1 (the second and the forth effects).

As known the quadrupole deformation β_2, having its minimal

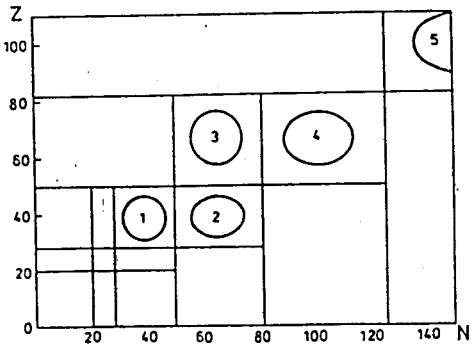

Fig. 5 Isotope chart in (N,Z) coordinates. The straight lines indicate shell closure, ovals - regions of deformed nuclei

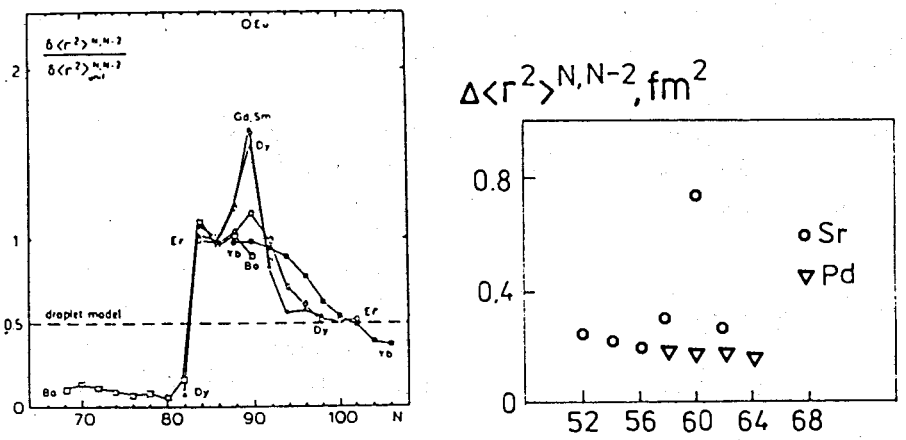

Fig. 6 Brix-Kopfermann plot of differential IS in the region of rare earths, normalized to the uniform shift. The value expected from the spherical droplet model is shown for comparison

Fig. 7 Plot of $\delta\langle r^2\rangle^{N,N-2}$ in the shape transition region around N = 60

value in nuclei with shell closure, increases with any deviation of N from the magic number. Corrections for β_2 according to eq. (1) work in direction of better agreement between theory and experiment [17]. Nevertheless, a coincidence has hardly been achieved. This would imply that the nuclear charge radius bears a much larger contribution from (probably) deformations higher order than offered from β_2 value alone. Another factor which cannot be excluded from a possible change of the nuclear charge distribution is the skin thickness. As shown by electron scattering experiments, the skin thickness is minimal for nuclei with neutron and proton shell closure and increases, when nucleons are added. The same phenomena are observed near closed proton shells as was mentioned in the foregoing section already.

2.4 Shape transition regions

As can be seen from the schematic nuclid chart in fig.5, there is a large number of transition regions: from shperical to deformed nuclei and vice versa. Due to systematic measurements in the last decade the shape transition regions have been investigated in extended isotopic chains:

i) transitions from spherical to deformed nuclei

N = 52 to 68	for	$_{37}Rb$, $_{38}Sr$, $_{46}Pd$
N = 84 to 98	for	all rare earths and $_{54}Xe$, $_{55}Cs$, $_{56}Ba$
N = 130 to 140	for	$_{88}Ra$, $_{90}Th$, $_{92}U$

ii) transitions from deformed to spherical nuclei

N = 39 to 48	for	$_{37}Rb$, $_{38}Sr$
N = 62 to 74	for	$_{54}Xe$, $_{55}Cs$, $_{56}Ba$, $_{60}Nd$
N = 101 to 112	for	$_{78}Pt$, $_{79}Au$, $_{80}Hg$

On the basis of this wide information a precise localization of the (N,Z) - points of the shape transitions was possible. Also the transition peculiarities for the different nuclid regions have been studied and related to the peculiarities of the corresponding nuclear structure (e.g. see review articles [8 ,17]).

In the present paper the discussion will be restricted only to

the case of the shape transition from spherical to deformed nuclei at N = 90. This is the region investigated in most detail: large number of investigated elements and long isotopic chains (see fig. 3). Moreover, we have also given some contributions to this area [18].

Local changes in the course of nuclear charge radii can be accentuated in a differential plot $\delta\langle r^2\rangle^{N,N-2}$, the so called Brix-Kopfermann plot [19]. By such plotting the step at the shape transition transformes into a needle (see fig. 5, covering a more extended N region than mentioned above). The plot reveals the following features:

- a drastic jump in $\delta\langle r^2\rangle^{N,N-2}$ beyond N=88 and for proton numbers Z around Z = 64 is observed;
- for even-even nuclei ($_{62}$Sm, $_{64}$Gd) the maximal value of $\delta\langle r^2\rangle^{N,N-2}$ is at N = 90; for odd-proton nuclei ($_{63}$Eu, $_{65}$Tb) - at N = 89;
- at either side of Z = 64 the $\delta\langle r^2\rangle^{88,90}$ value decreases, and the maximum in the curve completely vanishes.

The data presented in fig.5 are in an obvious correlation with the course of quadrupole deformation parameter β_2 [17] with increasing N: rapid increase between N = 88 and N = 90, i.e. just at the maximum of $\delta\langle r^2\rangle^{N,N-2}$, followed by a very slow increase beyond N = 92. Thus the analysis of the $\delta\langle r^2\rangle^{N,N-2}$ data in terms of eq.(1) seems to be justified. Moreover, as shown in [20], it permits to differentiate the changes of static from the changes of dynamic deformation around N = 90 by their influence on the variation of charge radii. At $N \geq 90$ (for odd nuclei $_{63}$Eu and $_{65}$Tb at $N \geq 89$) the static deformation dominates. At $N \leq 90$ the dynamic collective motion increases and both types of deformation are nearly equal. The odd isotopes of Sm with their extremely small static deformation are an exception.

In this way a high level of consistency is achieved only for the nuclei with smooth $\delta\langle r^2\rangle^{N,N-2}$ curves ($_{56}$Ba, $_{70}$Yb). However for nuclei with a sharp maximum at N = 90 this is not the case. If only quadrupole deformation is taken into account in eq. (1),

the calculated $\delta\langle r^2\rangle^{N,N-2}$ values are considerably larger than the experimental ones. The situation is significantly changed if octupole deformation is also included in the analysis. In the neutron region discussed, the octupole deformation at N < 90 decreases with increasing N, showing the most strong variation at the transition from N = 88 to N = 90; at N > 90, β_3 is nearly constant. Thus the β_3 contribution compensates the β_2 contribution and improves the consistency between calculated and expeerimental values.

The localization of the shape transition around Z = 64 has been emphasized by Casten et al.[21] on behalf of a systematics of energies of the 4^+ and 2^+ states in the ground state vibrational/rotational bands; it has been associated to the subshell closure at Z = 64.

Analogous pattern in the behaviour of ms charge radii is observed in the shape transition region $52 \leq N \leq 68$ (compare fig.6 and fig.7): the sharp jump in $\delta\langle r^2\rangle^{N,N-2}$ is located at N = 60 in the vicinity of the proton submagic number 38.

In contradiction to this case, very weak variation of the nuclear charge radius with neutron number is the main feature of its behaviour in all the three transition regions from deformed to spherical nuclei mentioned above (see fig.3). This is obviously due to the compensating influences of two different effects: a volume increase with increasing N and a decrease of the deformation when the nuclear shape tends to spherical. The unusually strong odd-even staggering at N < 108 in the case of $_{82}$Hg (fig.3) as well as in the cases of $_{78}$Pt and $_{79}$Au, has been related to a transition from small oblate to strong prolate deformation [8].

3. Nuclear charge radii changes of hafnium and titanium by laser spectroscopy

In the Flerov Laboratory of Nuclear Reactions, JINR, there are on going experiments on measurements of the changes in the ms charge radii and nuclear moments for two nuclei:

i) $_{72}$Hf, with average neutron number of about 107, which is

located closely beyond the well investigated rare earths in the very interesting mass region of strongly deformed nuclei;

ii) $_{22}$Ti, the stable isotopes of which lie within the very interesting shell $20 \leq N,Z \leq 28$; this is just in the Z region with a large lack of optical information on nuclear properties.

The experimental technique used has been described in [22]. Briefly, the light of a tunable cw dye laser is incident on a collimated atomic beam at a right angle. The laser excited resonance fluorescence is detected by a photomultiplier operating in a single photon counting mode. The spectra are recorded by a multichannel analyzer synchronized with the laser frequency tuning.

Hafnium and titanium are highly refractory elements for which the conventional method for production of an atomic beam by an electrically heated oven cannot be applied. In our experiments pulse laser evaporation was found to be the most convenient atomization method. For this purpose a Q-switched Nd:YAG laser (λ = 1.06 μm, pulse duration 10 ns, maximum energy in a pulse 50 mJ and repetition rate 12.5 - 100 Hz) was used. The optimal operating conditions included: a) suitable selection of the evaporation power density and b) synchronization between the laser pulses and registration electronics which ensured photon counting only when an atomic bunch was in the interaction region with the exciting laser beam.

3.1 Hafnium: results and discussion

All stable hafnium isotopes and its long living isotope ^{182}Hf ($T_{1/2} = 9 \times 10^6$ years) have been investigated. The ^{182}Hf was produced by a (γ,α) reaction in a metallic wolfram stopper of natural abundance at the microtron of FLNR, Dubna. It was stored in the stopper during many years of operation of the microtron. From this target a sample containing 10^{15} atoms of ^{182}Hf per nearly 1.5×10^{22} host W atoms, i.e. nearly 7×10^{-6} atomic percent, was prepared. In all cases a steady evaporation with sufficiently high yield of neutral atoms was obtained. The peak position of the ^{182}Hf resonance line relative to that of ^{180}Hf

was detected by a nearly three hours long free run laser scanning each of them of 1 s duration.

Measurements were made of the IS and hfs in three optical transitions found inside the spectral region of Rhodamin 6G (λ = 5719 Å, 5903 Å and 5946 Å). A "classical" way of semiempirical analysis using the well known Goudsmit-Fermi-Segre approximation was addopted to extract the nuclear parameter λ from the experimental IS. Then a well developed procedure [23] was applied to convert λ into ms radii changes.

Fig.8 displays the dependence of $\delta\langle r^2\rangle$ on the mass number A. The A region is extended by including the value of $\delta\langle r^2\rangle^{172,178} = -0.242(16)$ fm^2 from [24]. Fig.8 compiles also the results deduced from muonic atom spectra [25]. As can be seen, a discreapancy exists between the two sets of experimental data, exceeding the error limits. This is in contradiction to the most known cases of other nuclei, where optical and muonic atom results are not inconsistent within the experimental uncertainties [26] . Two peculiarities must be emphasized in the Hf case. On the one hand the optical data on $\delta\langle r^2\rangle$ from different authors agree very well, e.g. the present work values and those from [27]. We notice that these results are obtained (i) by investigating different optical transitions, and (ii) by using different methods of IS analysis no one containing callibration by muonic atom data. On the other hand electronic KX-ray data and muonic data are consistent with each other, but not with the optical $\delta\langle r^2\rangle$ values: for example $\delta\langle r^2\rangle^{180,178} = 0.103(7)$ fm^2 from X-ray [28],
$\delta\langle r^2\rangle^{180,178} = 0.106(7)$ fm^2 from muonic [25],
but $\delta\langle r^2\rangle^{180,178} = 0.075(4)$ fm^2 from our optical data.
The reason for this is unknown.

Finally, in Fig.8, plots of the spherical droplet model $\delta\langle r^2\rangle^{A,178}$ dependences with different sets of parameters [13, 29], demonstrating their influence on $\delta\langle r^2\rangle$, are drawn for comparison. It can be seen, that the general course of $\delta\langle r^2\rangle$ from muonic atom spectra coincides very well with the spherical droplet model prediction. Within the odd-even staggering the agreement is excellent, if droplet model parameters from [Be 85] are taken into account. Since the Hf isotopes belong to strongly

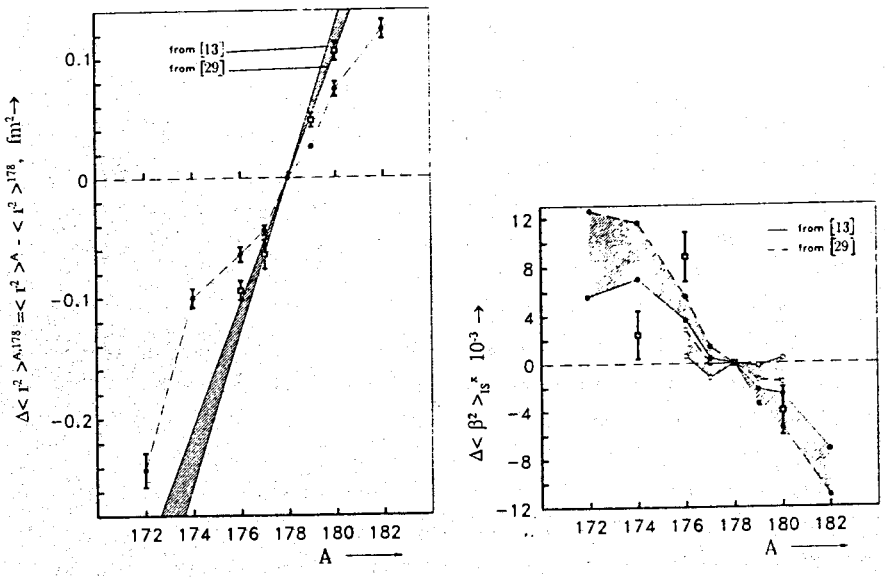

Fig. 8 $\delta\langle r^2\rangle^{A,178}$ versus the mass number A: • – our data; ∘ – the data from [24]; □ – muonic atom data [30]. The dashed region limits the possible variation of the spherical droplet model slope with changing the model parameters

Fig. 9 Course of $\langle\beta^2\rangle^A$ with respect to $\langle\beta^2\rangle^{178}$: • – isotope shifts data; ∘ – muonic atom data. Two different sets of droplet model parameters, denoted in the figure, are used. Values from B(E2)-measurements [15] with their error bars are given for comparison

deformed nuclei, this agreement means constant nuclear deformation in the investigated A region (see fig. 9, too). In the case of optical data the behaviour of $\delta\langle r^2\rangle$ is somewhat different: after a kink at A = 174 the experimental curve is nearly linear, but its slope is considerably smaller than the model slope. A fact which indicates a change of the deformation in the region A>174.

Thus, the optical and muonic data predict different behaviour of the nuclear deformation in the investigated Hf mass region.

This is explicitly shown in fig. 9: the deformation parameter $\langle\beta^2\rangle$ is calculated from the experimental $\delta\langle r^2\rangle$ values by using eq. (1) and with $\langle\beta_2\rangle^{178}$ as reference point. In fig. 9 the deformation parameters β_2^2 from B(E2)-values [15] are presented too. β_2^2 passes through a maximum at A = 176 , i.e. just in the middle between the two neutron magic numbers 82 and 126. These values lie closer to $\langle\beta^2\rangle$ from optical IS than from muonic atoms data. Nevertheless, in the first case some discrepancy exists, the main feature of which is the shift of the $\langle\beta^2\rangle$ maximum to a lower neutron number: N = 102.

For a correct explanation of the optical experimental results, higher order deformation should be taken into account. Unfortunately, systematic information on deformation parameters of Hf isotopes is not available. The only exceptions are: $\beta_3 = 0.093(29)$ for ^{176}Hf and $\beta_3 = 0.053(10)$ for ^{178}Hf [16]. Adding these values in eq. (1) leads to an increase of the observed discreapancy at A = 176. A smoothing influence should be expected, if one includes the hexadecapole deformation parameters predicted negative in the Hf mass region and with absolute values increasing with A [31, 32].

3.2 Titanium: results and discussion

The present paper reports on the changes of ms nuclear charge radii of Ti stable isotopes extracted from optical IS for the first time. The interpretation of the IS in light elements is subjected to two major difficulties:

i) The field shift is negligibly small within the experimental errors and the values of the IS are proportional to (A'- A)/A'A. Any deviation of the IS from this proportionality must be interpreted as an influence of the field shift. Thus, high accuracy measurements of IS are needed. To improve the experimental precision laser spectroscopic IS data on 5 spectral lines between $3d^24s^2\ a^3F(J = 0,1,2)$ and $3d^34p\ y^3D^o(J = 1,2,3)$ terms have been obtained. The values of $\delta\nu^{48,50}/\delta\nu^{46,48}$ ratios that we measured are systematically higher than the value 0.920 which is expected from the consideration of the mass effect only. The obtained ratio $\delta\nu^{48,50}/\delta\nu^{46,48} = 0.942(3)$ demonstrates without ambiguity the existence of a field effect.

ii) The specific mass shift is large and hard to allow for. The last is especially true in the 3d-optical series connected with the jump of 3d-electrons. For Ti, as well as for many other light elements, the use of muonic X- ray IS data seems to be the only feasible method for separating the large mass shift part and the much smaller field shift part of the optical IS. Muonic X-ray shifts however do not measure the same nuclear parameter as optical IS do, so that comparison of the optical IS with muonic X-ray shifts involves some uncertainties, the size of which is very difficult to estimated. For Ti this difficulty can be avoided, since muonic data can be combined with electronic scattering data in order to determine ms radii by a model independent analysis, yielding $\delta\langle r^2\rangle^{46,48} = -0.108(6)$ fm^2 and $\delta\langle r^2\rangle^{48,50} = -0.165(9)$ fm^2 [30]. With these values the SMS was deduced, and $\delta\langle r^2\rangle^{A,48}$ for all measured isotopes was determined. In this way we were able to predict the model independent ms radii of the stable odd-even Ti isotopes by a combined analysis [10 , 11] of two types of experimental data: model independent radii absolute values $\langle r^2\rangle$ from muonic atom data and model independent $\delta\langle r^2\rangle$ changes from the optical measurements.

The results are shown in fig.2. It should be noted here that in the investigated N region of Ti the IS show a similar shape as that of Ca; therefore it may be interpreted in the same lines (see section 2.2). A more detailed analysis of our results, as well as their discussion, are in progress.

4. Conclusion

The review on nuclear structure aspects of the charge radius variation shows that it is very sensitive to the model predictions and can serve as a probe for model validity.

The most conspicuous feature of the nuclear charge radius is the strong deviation from the prediction of the spherical droplet model requiring the inclusion of different multipolarity deformation effects (droplet model). An extension of the droplet model includes deformation effects using theoretical results on nuclear deformation, e.g. third order of quadrupole deformation, which discriminates between prolate and oblate shape, or a

generalization which includes thriaxial shape. The predictions on this basis are affected by corresponding uncertainties, but in general in many cases, even for long isotopic chains, an impressive coincidence is achieved.

Nevertheless, many experimental results require an alternative explanation. For light nuclei a variable skin thickness must be introduced to remove the observed discrepancies; for Z around and above Z = 82 modifications [Be 85] of the droplet model parameter can remove the problem to a large extend.

Acknowledgment Two of the authors (Marinova, Nadjakov) express their gratitude to the Bulgarian Ministry of Science and Education for financial support (grant F17).

References

1. C.W.de Jager, H.de Vries and C.de Vries, ADNDT, 14, 479 (1974)
2. H.de Vries, C.W.de Jager and C.de Vries, ADNDT 36, 495 (1987)
3. R.Engfer, H.Schneuwly, J.L.Vuilleumier, H.K.Walter and A.Zehnder, ADNDT 14, 509 (1974)
4. E.Wesolowski, J.Phys. G 10, 321 (1984)
5. M.S.Antony and J.Britz, Il Nuovo Cim. A 97, 255 (1987)
6. I.Angell, Acta Physica Hungarica 69, 233 (1991)
7. P.Aufmuth, K.Heilig and A.Steudel, ADNDT 37, 441 (1987)
8. E.W.Otten, in: Treatise on Heavy Ion Science, Nuclei far from Stability (Plenum Press, New York) 8, 517 (1989)
9. D.Kowalewska, K.Bekk, S.Goering, A.Goering, A.Hanser, W.Kaelber, G.Meisel, H.Rebel, Phys.Rev.A 44, R1442 (1991)
10. E.G.Nadjakov, Nuclear radii extended fit, unpublished (1992)
11. E.G.Nadjakov, K.P.Marinova and Yu.P.Gangrsky, ADNDT, 56, 133 (1994) , accepted for publication
12. V.S.Letokhov, V.I.Mishin, S.K.Sekatsky, V.N.Fedoseyev, G.D.Alkhazov, A.E.Barzakh, V.P.Denisov and V.E.Starodubsky, J.Phys. G 18, 1177 (1992)
13. W.D.Myers, K.-H.Schmidt, Nucl.Phys. A 410, 61 (1983)
14. P.Kleinheinz, J.Styczen, M.Piiparinen, J.Blomquist and M.Kortelahti, Phys.Rev.Lett. 48, 1457 (1982)
15. S.Raman, C.H.Malarkey, W.T.Milner, C.W.Nestor and P.H. Stelson, Atomic Data and Nuclear Data Tables 36, 1 (1987)
16. R.H.Spear, ADNDT, 42, 55 (1989)
17. Yu.P.Gangrsky, Particles & Nuclei -/б 1616 (1992)
18. S.K.Borisov, Yu.P.Gangrskii, Ch.Gradechny, S.G.Zemlyanoi, B.B.Krynetskii, K.P.Marinova, B.N.Markov, V.A.Mishin, Yu.Ts.Oganesyan, O.M.Stel'makh, Hoang Thi Kim Hue and Chan Kong Tam, Sov.Phys. JETP 66, 882 (1987)
19. H.Kopfermann, Nuclear Moments, Academic Press, New York, (1958)

20. G.D.Alkhasov, E.Ye.Berlovich, H.Wagner et al., Preprint LIAF 1006 (1984)
21. R.F.Casten, D.D.Warner, D.S.Brenner and R.L.Gill, Phys.Rev.Lett, 47, 1433 (1981)
22. Yu.P.Gangrsky, K.P.Marinova, B.N.Markov, E.G.Nadjakov, Yu.Ts.Oganessian, Han Gen I and Tran Kong Tam, Izv.Acad. Nauk USSR, Ser.Fiz. 49, 2261 (1985)
23. S.A.Ahmad, W.Klempt, R.Neugart, E.W.Otten, P.-G.Reinhard, G.Ulm and K.Wendt, Nucl.Phys. A 483, 244 (1988)
24. J.Rink, B.Gorski, W.Kaelber, G.Meisel, H.-J.Mielke, H.Rebel and M.Schubert, Z.Phys. A 342, 487 (1992)
25. Y.Tanaka, R.M.Steffen, E.B.Shera, W.Reuter, M.V.Hoehn and J.D.Zumbro, Phys.Rev. C 30, 350 (1984)
26. K.Heilig and A.Steudel, ADNDT 14, 613 (1974)
27. P.Aufmuth, I.Henneberg, A.Simiski and A.Steudel, Z.Phys. D 18, 107 (1991)
28. S.K.Bhattacherjee, F.Boehm and P.L.Lee, Phys.Rev. 188, 1919 (1969)
29. D.Berdichevsky and F.Tondeur, Z.Phys. A 322, 141 (1985)
30. H.D.Wohlfahrt, E.B.Schera, M.V.Hoehn, Y.Yamazaki and R.M.Steffen, Phys.Rev. C 23, 533 (1981)
31. P.Moeler and J.R.Nix, ADNDT 26, 165 (1981)
32. W.G.Nettles, A.V.Ramayya and J.H.Hamilton, J.Phys. G 14, L223 (1988)

Received by Publishing Department
on July 20, 1994.